# Calculations of CO Oxidation over a Au/TiO$_2$ Catalyst: A Study of Active Sites, Catalyst Deactivation, and Moisture Effects

Zhiyao Duan and Graeme Henkelman*

Department of Chemistry and the Institute for Computational Engineering and Sciences, The University of Texas at Austin, Austin, Texas 78712-0165, United States

**ABSTRACT:** The reaction mechanism of CO oxidation on Au/TiO$_2$ catalysts remains elusive. Here, we employ density functional theory calculations to gain an understanding of several important aspects of the system, including CO adsorption, the active oxygen species, catalyst deactivation, and the promoting effect of moisture on catalytic activity. Distinct from previous theoretical studies, which tend to address these questions individually, here we construct a model of the catalytic system which can address all of the issues mentioned. For this, we have considered the complex interactions among reactants, products, and catalysts under reaction conditions. The main findings of our present study are (1) the Au/TiO$_2$ interface boundary can be easily oxidized, (2) CO adsorption on oxidized Au results in the formation of O−Au−CO species, (3) surface lattice oxygen on a TiO$_2$ support is the active oxygen species, (4) CO$_2$ binds strongly on the O$_{top}$/Ti$_{5c}$ site, forming carbonate that blocks the active site, and finally (5) water can accelerate O$_2$ dissociation and carbonate decomposition. The results of our theoretical model are compared with existing experimental observations and found to be largely consistent with them.



CO oxidation on Au/TiO$_2$ reaction mechanism

active site          deactivation          moisture effect

**KEYWORDS:** *Au/TiO$_2$, moisture effect, carbonate formation, Mars−van Krevelen mechanism, CO oxidation, gold catalysis, heterogeneous catalysis, density functional theory*
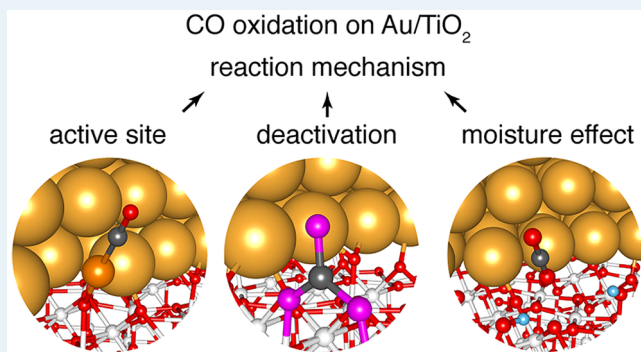
## INTRODUCTION

Gold nanoparticles (NPs) supported on titania (Au/TiO$_2$) are found to be surprisingly active for CO oxidation, even at low temperatures.[1] A large number of studies have been devoted to understanding the active sites and other factors controlling the activity of Au/TiO$_2$ catalysts.[2−10] O$_2$ activation is generally considered the key step for CO oxidation on the Au/TiO$_2$ catalyst because neither Au in its bulk form nor the TiO$_2$ support is able to activate O$_2$. The presence of under-coordinated atoms on Au NPs has been proposed as the primary factor for O$_2$ activation.[11−14] Over decades of studies, there is now greater consensus that the perimeter of the Au−TiO$_2$ interface contains the active site(s).[8,9,15] Widmann et al. found that the number of active oxygen species on Au/TiO$_2$ is linearly related to the number of perimeter sites at the Au−TiO$_2$ interface, indicating that the interfaces play a dominant role in O$_2$ activation.[16] A later contribution from the same group specifically identified lattice surface oxygen in the TiO$_2$ support as the active oxygen (O$_{act}$) species on the basis of the thermal stability of the functioning catalyst up to 400 °C.[17] A number of theoretical studies also highlighted the importance of perimeter sites for O$_2$ activation, although the assignment of O$_{act}$ varied among these studies from molecular oxygen to interfacial atomic oxygen to surface lattice oxygen.[18−30]

In fact, the O$_{act}$ or the active site for CO oxidation could be a dynamic concept and may only exist in operando when the catalyst is interacting with reactants and products under reaction conditions. In our recent theoretical study,[30] we found that O$_2$ can be readily activated and dissociated at the interfacial Au/Ti$_{5c}$ site due to synergistic effects between Au and the TiO$_2$ support, leading to easy oxidation of the Au−TiO$_2$ interface under reaction conditions. The adsorbed atomic oxygen at the Au/Ti$_{5c}$ site is reactive for CO oxidation. Furthermore, the oxidized interface also activates surface lattice oxygen atoms and renders them active for CO oxidation. Recently, a remarkable theoretical study, employing ab initio molecular dynamics, has also explored this possibility and discovered that a single Au atom can form dynamically and provide an active site for CO oxidation on Au/CeO$_2$ and Au/TiO$_2$.[28,31]

The nature of the active site is certainly important for understanding CO oxidation on Au/TiO$_2$, but there are other factors which are equally important, including catalyst deactivation and the effect of moisture. While understanding these effects is important for optimizing the catalyst performance, much less effort has been devoted to these other issues. The Au/TiO$_2$ catalyst has been found to gradually deactivate during CO oxidation.[32−34] The deactivation has been attributed

primarily to blocking of the interface perimeter as a result of carbonate formation; activity loss due to sintering of Au NPs was found to be only a minor issue. Moreover, the deactivation behavior is strongly dependent upon the pretreatment protocol. Recent work by Chandler et al. systematically compares different pretreatment effects on a commercial Au/TiO$_2$ catalyst.[33] They found a clear correlation between catalytic activity and the amount of surface carbonates produced in the reaction and established that the pretreatment protocol also determines the amount of surface carbonates deposited during the initial stage of CO oxidation. It was pointed out that harsh pretreatment conditions (longer time and/or higher temperature), in either a reducing or oxidizing environment, results in a catalyst that is easily deactivated by accumulating large amounts of carbonates. No pretreatment and mild treatments in a mixed H$_2$/O$_2$ environment lead to a catalyst with reduced carbonate formation and higher steady-state activity.

Water, in the reactant mixture for CO oxidation, was found to enhance the activity of the Au/TiO$_2$ catalyst.[10,35−40] There are two proposed mechanisms for the moisture effect: first it facilitates O$_2$ activation, and second, it accelerates decomposition of the reaction-inhibiting surface carbonates. The water-facilitated O$_2$ activation is proposed to be via OOH formation.[36,37,40] Water molecules can also transform carbonates into bicarbonates to accelerate decomposition, as proposed in several studies.[10,35] A recent study using kinetic isotope analysis and in situ infrared spectroscopy demonstrated that O−H bond breaking is involved in the rate-determining step (RDS).[39] Supporting density functional theory (DFT) calculations proposed that proton transfer is involved in COOH decomposition.

In a previous theoretical study, we focused on O$_2$ activation on the Au/TiO$_2$ catalyst.[30] Here, to address the numerous aspects of CO oxidation on Au/TiO$_2$ observed experimentally, we extend our previous work to the full reaction cycle of CO oxidation. Our study simultaneously considers the active site, catalyst deactivation, and moisture effects, so that these three major factors can be understood in terms of a single reaction pathway. The results of our calculations are compared with existing experimental observations, and our model is generally in agreement with them.

## ■ COMPUTATIONAL METHODS

Plane-wave-based spin-polarized DFT calculations were performed using the Vienna ab initio simulation package.[41−43]

The generalized gradient approximation with the Perdew−Wang (PW91) functional[44] was used to describe the exchange and correlation energy. Electron−ion interactions were treated within the projector augmented wave framework.[45] In all calculations, the energy cutoff of the plane wave basis set was 400 eV. The DFT+$U$ method was applied to 3d orbitals of Ti to correct the on-site Coulomb interactions.[46] The value of $U_{eff}$ was chosen to be 4.0 eV to reproduce the electronic structure that has been observed experimentally.[47,48] Due to the large structural model employed, a Γ-point sampling of the Brillouin zone was found to be sufficient for calculating the total energy of the system. Optimized structures were obtained by minimizing the forces on each ion until they fell below 0.05 eV/Å. Transition states were determined with the climbing image nudged elastic band method.[49,50] A Bader analysis was employed to determine the local charge of atoms in the system.[51−53] Additional details and discussion of our atomic model are given in ref 30. Briefly, the interface between a TiO$_2$

surface and a supported Au nanoparticle is modeled by a periodic one-dimensional Au rod deposited along the TiO$_2$ [1$\bar{1}$0] direction of a rutile TiO$_2$(110) slab. The Au rod contains three layers; the interfacial layer has the structure of the Au(111) surface. In order to minimize the strain, a long Au rod consisting of seven Au atoms along the [1$\bar{1}$0] direction is used. The lattice constants calculated in this work are $a$ = 4.17 Å for fcc Au and $a$ = 4.69 Å, $c$ = 3.03 Å for rutile TiO$_2$. On the basis of these lattice constants, the Au rod is compressed by 3.7% in the axial direction to be commensurate with the $p(5 \times 3)$ TiO$_2$(110) substrate in the [1$\bar{1}$0] direction. The TiO$_2$ substrate contains three stoichiometric TiO$_2$ layers. The top TiO$_2$ layer is allowed to relax while the bottom two layers are fixed in bulk lattice positions.

## ■ RESULTS

**O$_2$ Activation at the Au/Ti$_{5c}$ Site.** In our previous study of O$_2$ activation at the Au−TiO$_2$ interface boundary,[30] we found that O$_2$ is readily activated and dissociated at the interfacial Au/Ti$_{5c}$ site. The activation energy for O$_2$ dissociation at this site is 0.5 eV, which is easily overcome at room temperature. We have further shown, due to facile O$_2$ dissociation, that the Au−TiO$_2$ interface boundary can be easily oxidized. Atomic oxygen atoms, adsorbed at the interfacial Au/Ti$_{5c}$ sites, were found to play an important role in CO oxidation catalysis. First, they can directly react with a CO molecule adsorbed nearby on a Au atom with an activation energy as low as 0.22 eV. Second, an oxidized interface boundary can lower the energy cost for oxygen vacancy formation, thus making surface lattice oxygen atoms (O$_{bri}$) active for CO oxidation reaction. Here, we extend this model by considering CO adsorption on various Au sites with metallic, cationic, and anionic charge states.

**CO Adsorption and the Formation of Cationic Au Carbonyl Species.** CO binding energies were evaluated on various Au sites on the Au rod/TiO$_2$ model. The CO adsorption configurations are shown in Figure 1. The binding
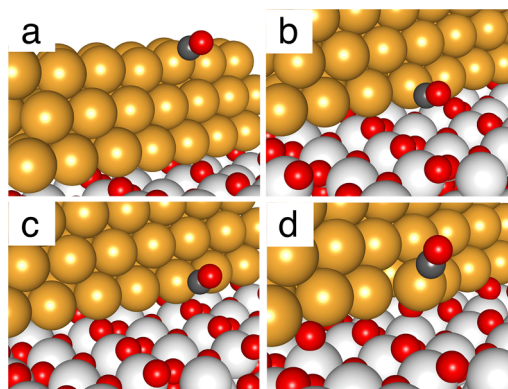


**Figure 1.** Structures of CO adsorption on various Au species on the Au/TiO$_2$ catalyst. The adsorption sites include (a) Au rod edge, (b) Au/Ti$_{5c}$, (c) Au/Ti$_{6c}$, and (d) Au/O$_{top}$.

sites considered include an undercoordinated Au atom at the edge of the Au rod (Figure 1a), a Au atom above a Ti$_{5c}$ at the stoichiometric interface boundary (Figure 1b), a Au atom sitting above an O$_{bri}$ at the stoichiometric interface boundary (Figure 1c), and a Au atom binding with O$_{top}$ at the oxidized interface boundary (Figure 1d). The four Au sites are denoted as Au edge, Au/Ti$_{5c}$, Au/O$_{bri}$, and Au/O$_{top}$, respectively. Table 1 summarizes the calculated CO binding energies at these sites.

**Table 1. Details of CO Adsorption at Various Binding Sites$^a$**

| site | structure | Au charge (e) | $r_{CO}$ (Å) | $\nu_{CO}$ (cm$^{-1}$) | $E_{bind}^{CO}$ (eV) |
|------|-----------|---------------|--------------|------------------------|----------------------|
| gas phase | | | 1.142 | 2130 (2143) | |
| Ti$_{5c}$ | | | 1.139 | 2147 (2160) | −0.29 |
| Au edge | Figure 1a | −0.03 | 1.148 | 2070 (2083) | −0.83 |
| Au/Ti$_{5c}$ | Figure 1b | −0.07 | 1.150 | 2043 (2056) | −0.67 |
| Au/O$_{bri}$ | Figure 1c | 0.14 | 1.147 | 2071 (2084) | −0.46 |
| Au/O$_{top}$ | Figure 1d | 0.25 | 1.149 | 2100 (2113) | −1.31 |

$^a$The $\nu_{CO}$ values in parentheses include a 13 cm$^{-1}$ correction for systematic errors in the DFT-calculated CO vibrational frequencies.

Along with the binding energies, Bader charges of the Au species at the binding site, C−O bond lengths, and vibrational frequencies of C−O bonds are also given. Data for the gas-phase CO molecule and the CO adsorbed atop the Ti$_{5c}$ site on the TiO$_2$ support are included for comparison.

First, we note that CO adsorbs more strongly on Au sites than on the TiO$_2$ support, which is expected.[54] It is surprising, however, that CO adsorbs most strongly on the Au/O$_{top}$ site at the oxidized interface boundary with a binding energy of −1.31 eV, rather than the most commonly considered under-coordinated Au site, with a binding energy of −0.83 eV. CO adsorption on the Au/O$_{top}$ site adopts an interesting structural motif, in which O$_{top}$−Au−CO forms a linear molecular species, in analogy to the gold monocarbonyl chloride (Au(CO)Cl) complexes reported more than 90 years ago.[55] Upon formation of the O−Au−CO species, the Au atom is pulled out of the matrix of the Au rod. A consequence of Au carbonyl formation is the cationic nature of Au. Before CO adsorption, the Au atom has a positive Bader charge of 0.25 e due to its interaction with the O$_{top}$ atom. CO adsorption on anionic Au/Ti$_{5c}$ and slightly cationic Au/O$_{bri}$ sites have even weaker binding strengths of −0.67 and −0.46 eV, respectively.

Despite having a stronger binding strength, the CO molecule in the O−Au−CO species has a higher $\nu_{CO}$ value and shorter C−O bond length in comparison to CO molecules adsorbed on other Au sites. This phenomenon is well-known in cationic metal carbonyl complexes[56] and has been attributed to an electrostatic effect: the electric field caused by the cationic Au induces charge transfer from O to C, diminishing the polarization of the CO molecule and thereby increasing covalency.[57] A recent theoretical study further elaborated upon this explanation by taking into account the interplay between the electrostatic effect and π back-donation. The two effects shift charge in opposite directions so the net direction of the polarization of π CO bonding orbital determines whether the CO bond is strengthened or weakened.[58] Experimentally, CO adsorption on cationic Au species has been identified by vibrational spectroscopy.[56] We will compare the calculated $\nu_{CO}$ values with experimental observations later in the paper. Note that our DFT simulations underestimate $\nu_{CO}$ for the free CO molecule by −13 cm$^{-1}$ (calculated 2130 cm$^{-1}$ vs experimental 2143 cm$^{-1}$),[59] and this systematic shift will be applied when making comparisons to experiment.

The formation of O−Au−CO complexes has important consequences for CO oxidation catalysis. First, it provides strong binding sites for CO molecules close to the interface, where O$_{act}$ species are located. Hence, the availability of CO is enhanced, especially at high temperatures, and diffusion of CO molecules from the Au edge to the interface boundary is not required for CO oxidation. Moreover, our previous proposal of Au/O$_{top}$/Ti$_{5c}$ being the O$_{act}$ needs to be revised. After O−Au−CO species formation, Au/O$_{top}$/Ti$_{5c}$ is no longer accessible to the adsorbed CO molecule in O−Au−CO. As a result, Au/O$_{top}$/Ti$_{5c}$ is not active for CO oxidation, at least at low temperatures, and the oxidized interface boundary cannot be reduced in a CO oxidation reactive environment.
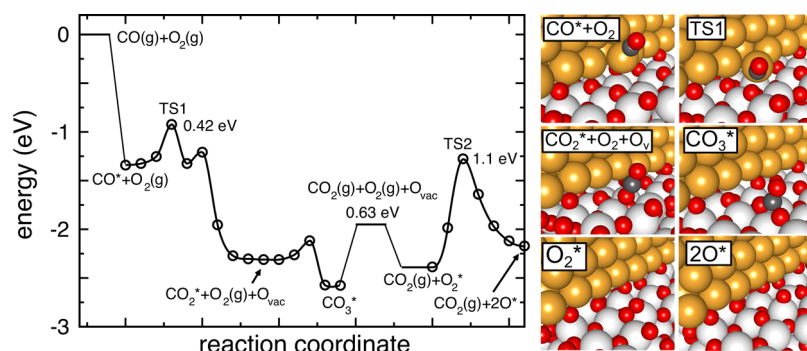
**Reaction Mechanism of CO Oxidation.** Figure 2 shows the potential energy surface (PES) of O$_2$ dissociation and the subsequent CO oxidation process that removes the O$_{top}$ species present from O$_2$ dissociation. The barrier for adsorbed CO to react with O$_{top}$ is 0.5 eV, which indicates that the removal of O$_{top}$ near the interface boundary is a facile process at room temperature. As a result, the interface perimeter is available for further CO oxidation.

We further examined how the O−Au−CO species reacts with O$_{act}$ for CO$_2$ production. Depending upon the source of O$_{act}$, the reaction can be classified as following teither he Langmuir−Hinshelwood (LH) mechanism or the Mars−van Krevelen (MvK) mechanism. In the LH mechanism, adsorbed O$_2$ is the oxidant that reacts with adsorbed CO. In the MvK mechanism, the active O species is the surface lattice O (O$_{bri}$). As discussed above, formation of the O−Au−CO species leads to an unreducible Au−TiO$_2$ interface where O$_2$ adsorption on the TiO$_2$ surface is inhibited because no available electron is able to transfer to the adsorbed O$_2$.[30] The O$_2$ at the CO adsorbed oxidized interface indeed tends to desorb from the TiO$_2$ surface. Consequently, the only possible mechanism at the Au−TiO$_2$ interface boundary is the MvK mechanism.

The calculated PES and the atomic structures for key intermediates following the MvK mechanism are shown in Figure 3. First, the adsorbed CO approaches an O$_{bri}$, forming a bent CO$_2$ molecule with an energy barrier of 0.42 eV. The bent
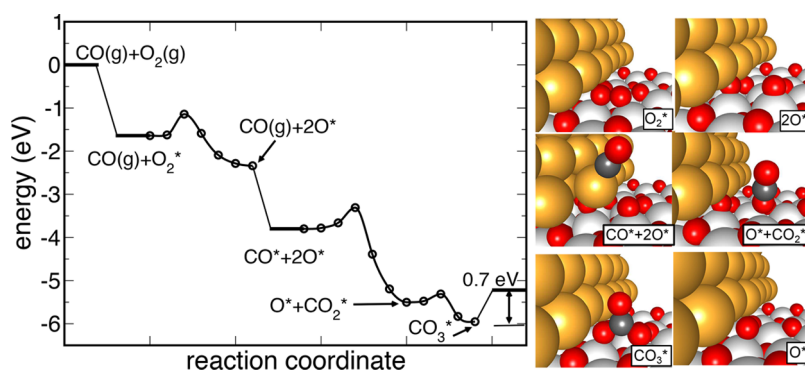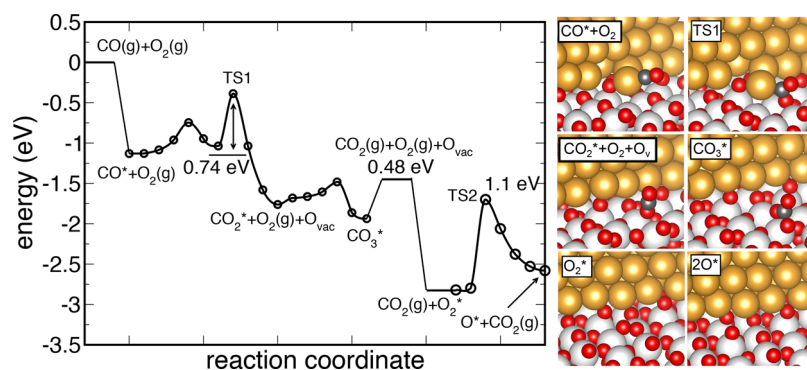


**Figure 2.** O$_2$ dissociation and initial CO oxidation step at the Au−TiO$_2$ interface boundary.

**Figure 3.** Reaction pathway of CO oxidation at the oxidized Au−TiO$_2$ interface boundary following the Mars−van Krevelen reaction mechanism.
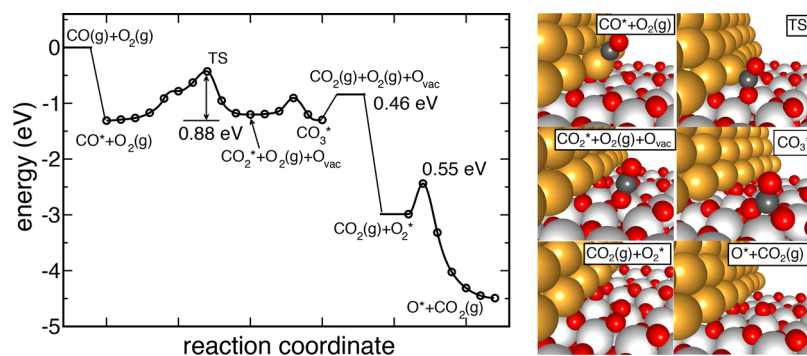


**Figure 4.** Reaction pathway of CO oxidation at a near-stoichiometric Au−TiO$_2$ interface boundary following the MvK reaction mechanism.



**Figure 5.** Reaction pathway of CO oxidation at the Au−TiO$_2$ interface boundary with an O vacancy underneath the Au rod, following the MvK reaction mechanism.

CO$_2$ then easily transforms into a linear CO$_2$ species adsorbed at the oxygen vacancy site. The energy is further decreased by −0.3 eV when the adsorbed CO$_2$ bends as it interacts with an O$_{bri}$ to form an absorbed CO$_3$ molecule. The CO$_3$ molecule subsequently decomposes to CO$_2$, leaving an oxygen vacancy on the TiO$_2$ surface in a process that is endothermic by 0.63 eV. The entire CO$_2$ formation process is facile, as the highest energy barrier is only 0.42 eV, which is associated with the formation of the bent CO$_2$ species. The desorption of CO$_2$ costs more enthalpy, but it is readily compensated by the entropy of gas-phase CO$_2$ at room temperature. The surface oxygen vacancy can then be refilled by O$_2$ adsorption and dissociation in a process that is highly activated with an energy barrier of 1.1 eV, due to the destabilization of O$_{bri}$ at the oxidized interface. The resulting O$_{top}$ readily reacts with another O−Au−CO species with an energy barrier of 0.5 eV (not shown in Figure 3) to complete the reaction cycle. The

rate-determining step (RDS) of the MvK mechanism is then the O$_2$ dissociation at the oxidized Au−TiO$_2$ interface.

It is interesting to compare the MvK mechanism at the near-stoichiometric Au−TiO$_2$ interface with that at the oxidized Au/TiO$_2$ interface, which was just discussed. At the near-stoichiometric interface, only one oxygen is adsorbed at the oxidized interface, instead of six. The PES following the MvK mechanism at the near-stoichiometric interface is shown in Figure 4. In contrast to CO oxidation at the oxidized interface, the formation of a bent CO$_2$ molecule now requires an energy barrier of 0.88 eV: much higher than the 0.42 eV barrier at the oxidized interface. Moreover, the dissociation of O$_2$ adsorbed at the surface oxygen vacancy requires a barrier of only 0.55 eV. Both observations illustrate the role that the oxidized interface plays in facilitating CO$_2$ formation at the cost of O$_2$ activation for the MvK mechanism.

Au NPs tend to nucleate on oxygen vacancies present in the oxide support due to a stronger adsorption energy. To consider

the effect of oxygen vacancies on the reaction mechanism, we created an oxygen vacancy underneath the Au rod. In this model, the facile $O_2$ activation at the interface and interfacial oxidation remain the same as in the stoichiometric model. When the interface is oxidized, $O_2$ cannot adsorb on the $TiO_2$ support, which then leaves the MvK mechanism as the only available pathway. The PES of the MvK mechanism is shown Figure 5. The rate-determining step is still $O_2$ dissociation, here with a barrier of 1.1 eV. Thus, the presence of the oxygen vacancy does not alter the mechanism of CO oxidation that we previously discussed for the nondefective model.

**CO- and H$_2$O-Facilitated O$_2$ Dissociation.** The highly activated $O_2$ splitting process at the oxidized interface inhibits the reaction cycle of CO oxidation at low temperature. In the following, we examine two possible ways of facilitating $O_2$ dissociation.

The first is CO-facilitated $O_2$ activation, in which the adsorbed CO in the O−Au−CO species reacts directly with one of the oxygen atoms in the $O_2$ molecule, so that the energy cost of O−O bond scission is compensated by the energy gain of C−O bond formation. After the proposed reaction pathway is relaxed, it splits into two parts: $O_2$ first dissociates, and then CO reacts with the resulting $O_{top}$. The PES of $O_2$ dissociation in the presence of O−Au−CO at the oxidized interface is shown in Figure 6a. The energy barrier is decreased from 1.1 to



**Figure 6.** Potential energy of O−O bond splitting at an oxygen vacancy in the presence of CO and water: (a) CO facilitated; (b) water facilitated; (c) both CO and water facilitated.

0.69 eV, which can be attributed to the attractive interaction between the $O_2$ molecule and the Au atom in O−Au−CO. The remaining process of CO attacking $O_{top}$ requires a barrier of only 0.5 eV.

We examined the influence of moisture on the barrier of $O_2$ dissociation. A water molecule adsorbs most strongly atop $Ti_{5c}$ sites on the $TiO_2$ surface, with a binding energy of −1.2 eV. The adsorbed water, however, has weak interactions with $O_2$ adsorbed at an adjacent oxygen vacancy due to the long distance (3.0 Å) between them. We have conducted NEB calculations of OOH formation in the presence of water adsorbed at the atop $Ti_{5c}$ site. The converged reaction path favors splitting the O−O bond first rather than OOH formation, so that there is no reduction in the energy barrier. While the water molecule can easily dissociate on the $TiO_2$ surface to form $OH/Ti_{5c}$ and $H/O_{bri}$, we find that the water molecule can adsorb at the $H/O_{bri}$ site with an appreciable binding energy of −0.8 eV due primarily to an electrostatic interaction. The adsorption structure is shown in Figure 6b. In this configuration, the H atom in the water molecule is only 1.6 Å from one of the O atoms in the adsorbed $O_2$ molecule. The adsorbed $O_2$ can be converted to OOH through a concerted H shuffling mechanism, in which adsorbed $O_2$ abstracts a hydrogen atom from water to form OOH; simultaneously the water molecule regains a hydrogen atom from $H/O_{bri}$. The process is equithermic with a low barrier of only 0.1 eV. Subsequently, the OOH molecule can dissociate into O and OH fragments with an energy barrier of 0.68 eV, as shown in Figure 6b. Hence, the presence of water adsorbed on $H/O_{bri}$ can facilitate O−O dissociation through the generation of an OOH intermediate. OOH dissociation can be facilitated by a nearby adsorbed CO molecule in a process shown in Figure 6c. The barrier of the OOH splitting process drops to 0.5 eV as a result of the adsorbed OH, forming an additional bond with the Au atom in the O−Au−CO species.

**Catalyst Deactivation and Regeneration.** $O_2$ splitting at an oxygen vacancy results in filling of the oxygen vacancy and the generation of an adsorbed $O_{top}$. The adsorbed $O_{top}$ is very active and can oxidize CO with a barrier of 0.5 eV. Alternatively, the resulting $CO_2$ can bind strongly on the atop O to form a carbonate molecule, $CO_3$, with a binding energy as low as −1.50 eV. We have examined four $CO_2$ adsorption structures at the perimeter of Au−$TiO_2$ interface as shown in Figure 7, including a bidentate Ti structure, a monodentate Ti structure, a bidentate $Au^0Ti$ structure, and a bidentate $Au^{\delta+}Ti$ structure. The characteristic vibrational frequencies of these carbonates have been calculated and will be compared with experimental data in the next section. Taking the entropy of gas-phase $CO_2$ into account, the $CO_2$ desorption process would only be favorable above 600 K.[60] Such a high binding strength of $CO_2$ on $O_{top}$ would lead to catalyst deactivation, since the active sites along the interface boundary will be blocked by adsorbed carbonates.

We find the presence of water in the system will result in bicarbonate ($CO_3H$) formation, which will greatly alleviate the catalyst deactivation caused by $CO_3$ adsorption. The process of $CO_3H$ formation and $CO_2$ desorption is shown in Figure 8. It can be seen that the barriers for water dissociation and hydrogen migration on the $TiO_2$ surface are very low. The attachment of H to the $CO_3H$ molecule is an endothermic process, requiring an energy barrier of 0.4 eV. $CO_2$ desorption is also an endothermic process, but the heat of reaction is reduced significantly to 0.6 eV. The energy cost of this process
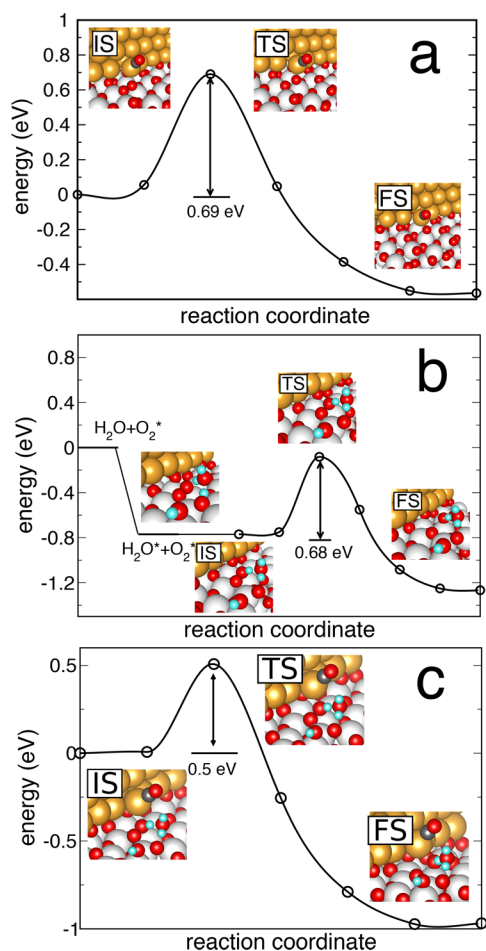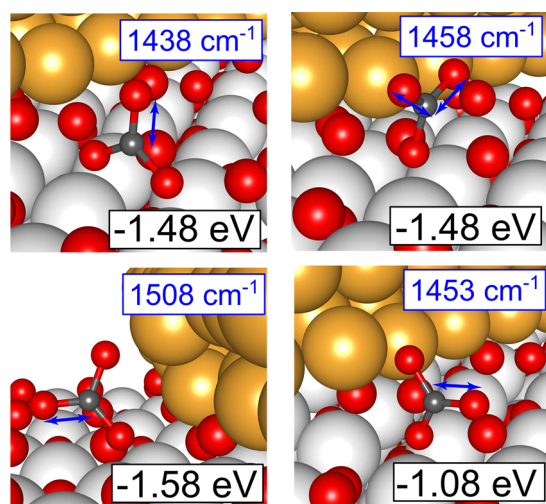
**Figure 7.** $CO_3$ molecules adsorbed at the perimeter of the oxidized Au−$TiO_2$ interface. The values in black are the binding energies of $CO_2$ molecules on $O_{top}$ sites. The values in blue are characteristic vibrational frequencies. The corresponding vibrational modes are indicated by the arrows.

is easily compensated by the entropy of gas-phase $CO_2$ at room temperature. Thus, the most difficult step for $CO_2$ desorption is the formation of $CO_3H$, at room temperature.

**Comparison with Experiments.** The formation of O−Au−CO species has been observed in several spectroscopic studies.[61−64] A comprehensive review of these studies can be found in ref 56. In these studies, infrared (IR) vibrational bands at ∼2100 $cm^{-1}$ were assigned to CO adsorbed on metallic Au ($Au^0$). The experimental vibrational frequency of CO−$Au^0$ is somewhat higher than the calculated value of 2080 $cm^{-1}$ of CO adsorbed at the edge of the Au rod (note that all calculated frequencies have been shifted by 13 $cm^{-1}$ to reproduce the gas-phase CO reference). We attribute the modest underestimation of the calculated CO−$Au^0$ vibrational frequency to the low CO coverage in our simulation in comparison to experiment. When the Au/$TiO_2$ catalyst was exposed to both CO and $O_2$, it was found that a new band appears at 2120 $cm^{-1}$, which was assigned to CO adsorbed on oxidized Au.[61−64] Experimental assignment of this species varies from CO−$Au^{\delta+}$−$O_2^{\delta-}$[61,62] to CO−$Au^{\delta+}$−$O^{\delta-}$.[63] These experimental observations are consistent with our simulation showing the formation of an O−Au−CO species, whose $\nu_{CO}$ value is calculated to be 2113 $cm^{-1}$, at the oxidized Au−$TiO_2$ interface boundary. The difference between the calculated and the experimental frequencies of CO−$Au^{\delta+}$−$O^{\delta-}$ can be explained by the difference in Au oxidation state (different $\delta+$) between

simulation and experiment. An experimental study found that a band is present at 2119 $cm^{-1}$ when both CO and $O_2$ are introduced; switching the CO source off and leaving air flowing shifts the band further to 2125 $cm^{-1}$.[63] In that study, the CO adsorption on $Au^{\delta+}$ was found to be much stronger than that on $Au^0$ since it cannot be removed even on purging for 60 min, which supports our calculation that Au/$O_{top}$ provides a very strong binding site for CO. We have also examined the possibility of assigning the vibrational band to the CO−$Au^{\delta+}$−$O_2^{\delta-}$ species. The resulting $\nu_{CO}$ value is as low as 2075 $cm^{-1}$, similar to that for CO adsorbed on anionic Au, since the adsorbed $O_2$ at the Au/$Ti_{5c}$ site receives electrons from the support. With regard to the role of O−Au−CO in CO oxidation, in situ Fourier transform infrared spectroscopy (FTIR) revealed that the CO species corresponding to the band at 2112 $cm^{-1}$ slowly disappears at −60 °C.[64] At this low temperature, however, CO adsorbed at metallic Au, corresponding to the band at 2090 $cm^{-1}$, was found to be more active in the same study. At higher temperatures of 273 K, the O−Au−CO species was proposed as a very reactive intermediate for CO oxidation.[36]

The assignment of the reaction mechanism (LH vs MvK) and $O_{act}$ for CO oxidation are controversial in experimental studies. Here, we pay particular attention to the recent work of Behm et al. based on pulse experiments performed in a temporal analysis of products (TAP) reactor under reaction conditions at room temperature and above.[15−17,65] These experiments are extremely sensitive to the oxygen consumption and $O_{act}$ formation of an amount of only 1% of the total oxygen coverage on the catalyst surface. First, regarding the location of the active O species, it was found that the cumulative amount of $CO_2$ increased linearly with the Au−$TiO_2$ interface perimeter length by studying Au/$TiO_2$ catalysts containing Au nanoparticles of different sizes.[9,16] Subsequent work further resolved that the lattice oxygen atoms on the $TiO_2$ surface at the interface perimeter are the active O species due to superior stability and nonactivated replenishment, consistent with a Au-assisted MvK mechanism.[17] These conclusions are consistent with our proposed mechanism, as discussed further above. In situ electrical conductance measurements also demonstrated the formation of surface oxygen vacancies at Au−$TiO_2$ perimeter sites during CO oxidation.[66] The Au-assisted MvK mechanism is influenced by reaction temperature.[65] When the TAP reactor results are combined with electron paramagnetic resonance spectroscopy, it is shown that CO oxidation, following the MvK mechanism, readily takes place at 120 °C; it remains active at −20 °C and only completely shuts down at −90 °C. Our simulation results are in agreement with these experiments in that there are sizable energy barriers, typically
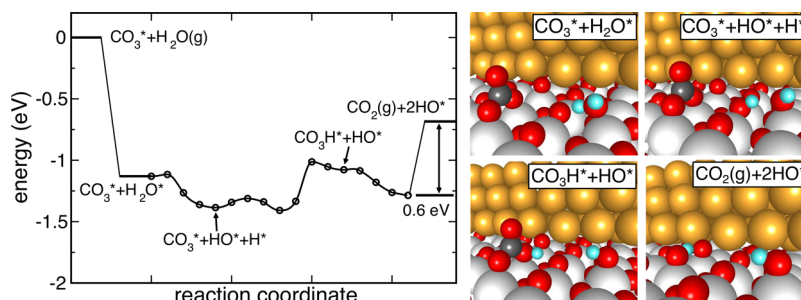


**Figure 8.** Transformation of $CO_3$ to $CO_3H$ in the presence of water.

with a magnitude of ∼0.5 eV along the reaction pathways we proposed above. These barriers cannot be overcome at low temperatures. The reaction mechanism at low temperatures could only involve CO and $O_2$ adsorbed on $Au^0$ following a LH mechanism as discussed in the aforementioned in situ FTIR study.[64] Above room temperature, the dominant mechanism should be the MvK mechanism, since CO adsorption and especially $O_2$ adsorption are very weak on metallic Au, rendering the LH mechanism unfavorable. Although the evidence for the MvK mechanism and the active role of the support are evident in the experiments discussed above and in our calculations, a recent study has demonstrated that colloidal Au (∼3.8 nm in size) can catalyze CO oxidation without any support.[67] For now, it is not clear to us how Au NP can activate $O_2$ on its own. This is clearly a direction for further research, particularly as a challenge for theory.

Experiments have shown that carbonate accumulates during the reaction at the interface boundary, leading to catalyst deactivation.[32−34] We also observed that $CO_2$ adsorbs strongly on $O_{top}$ with a calculated binding energy of −1.5 eV, which will cause $CO_3$ accumulation below 600 K. The carbonates deposited on the catalysts have been demonstrated to exhibit two major in situ diffuse reflectance infrared Fourier transform spectroscopy peaks at around 1500 and 1400 cm$^{-1}$. Our calculated vibrational frequencies of adsorbed carbonates are in agreement with these experimental data. According to our calculations, the peak observed at 1500 cm$^{-1}$ is tentatively assigned to the carbonates adsorbed at bidentate $Au^0$Ti sites.[34] The peak at 1400 cm$^{-1}$ is attributed to carbonates adsorbed in monodentate Ti and bidentate Ti configurations on the $TiO_2$ support. The $O_{top}$ species coming from the $O_2$ dissociation on the surface oxygen vacancy plays a key role in trapping $CO_2$. We use this simulation result to explain the experimental observations that pretreatment conditions significantly affect catalyst deactivation.[33] It has been shown that pretreatment of $Au/TiO_2$ in pure $H_2$ or an $O_2$ environment results in catalyst deactivation. Pretreatment in mixed $H_2$ and $O_2$ or no pretreatment results in only mild deactivation. We attempt to explain this observation by arguing that both pure $O_2$ and $H_2$ will lead to a high concentration of $O_{top}$ on the $TiO_2$ surface. In a pure $O_2$ environment at high temperatures, there would be more $O_2$ dissociation at the interface perimeter. On the other hand, in pure $H_2$, the pretreatment would leave a high concentration of surface oxygen vacancies that induce more $O_2$ dissociation on exposure to the reactant gas mixture.

Although the moisture effect in promoting CO oxidation on $Au/TiO_2$ catalyst is evident,[35,36,39] the explanation for it varies between reports. Four major proposed mechanisms of the moisture effect were recently summarized in a review by Haruta.[10] The proposed mechanisms include creation of cationic gold, direct participation in $CO_2$ formation, activation of $O_2$, and transformation and decomposition of carbonate species. Our simulation results show that water can play two roles in CO oxidation on the $Au/TiO_2$ catalyst. First, water present in the catalyst can lead to OOH formation, which will reduce the barrier for $O_2$ dissociation on the oxidized $Au/TiO_2$ catalyst. Second, water can convert adsorbed carbonate to bicarbonate, which weakens the binding strength of $CO_2$ and alleviates the poisoning effect of carbonate. The effect on $O_2$ activation can also be accomplished by CO-assisted O−O bond breaking as discussed above. Hence, we find the most important role of water to be transforming surface carbonates to bicarbonates, a conclusion that is consistent with experi-

ments.[35,36] The moisture effect was determined to have a strong H/D kinetic isotope effect (KIE) of ∼2, which indicates that the O−H bond breaking is involved in the rate-determining step (RDS).[39] According to our simulation, the step that could lead to strong KIE is proton transfer from H−$O_{bri}$ to $CO_3$, which has a barrier of 0.4 eV.

## ■ CONCLUSIONS

Here, we employed DFT simulations to gain insight into several important yet elusive issues related to catalytic CO oxidation over $Au/TiO_2$, including the active oxygen species, the mechanism of catalyst deactivation and regeneration, and the effects of moisture. We found that $O_2$ can be easily activated at the interface boundary, which leads to an oxidized interface. CO interacts strongly with the oxidized interface to form O−Au−CO species. The oxidized interface also activates lattice oxygen in $TiO_2$ as a result of electron transfer from $Ti^{3+}$. Adsorbed CO molecules can subsequently react with lattice oxygen in the support following the MvK mechanism, with a low barrier of 0.4 eV. The resulting surface oxygen vacancy can be filled with a dissociating $O_2$ molecule; however, this is a highly activated process with a barrier of 1.1 eV. In addition, a stable carbonate species forms on the $TiO_2$ support as a result of $CO_2$ adsorption on active oxygen atoms adsorbed atop Ti atoms, which would lead to catalyst deactivation. Our calculations show that both difficulties can be overcome by introducing water in the reactant feed. For $O_2$ activation, the barrier for O−O bond splitting is lowered by 0.4 eV as a result of OOH formation and $CO_3$ can be converted to a bicarbonate species which significantly reduces the $CO_2$ heats of desorption from 1.5 to 0.6 eV.

## ■ AUTHOR INFORMATION

**Corresponding Author**
*E-mail for G.H.: henkelman@utexas.edu.
**ORCID** 
Graeme Henkelman: 0000-0002-0336-7153
**Notes**
The authors declare no competing financial interest.

## ■ ACKNOWLEDGMENTS

## ■ REFERENCES

(1) Haruta, M.; Kobayashi, T.; Sano, H.; Yamada, N. *Chem. Lett.* **1987**, *16*, 405−408.
(2) Haruta, M. *CATTECH* **2002**, *6*, 102−115.
(3) Bond, G. C.; Thompson, D. T. *Catal. Rev.: Sci. Eng.* **1999**, *41*, 319−388.
(4) Hashmi, A. S. K.; Hutchings, G. J. *Angew. Chem., Int. Ed.* **2006**, *45*, 7896−7936.
(5) Bond, G. C.; Thompson, D. T. *Gold Bull.* **2000**, *33*, 41−50.
(6) Haruta, M.; Daté, M. *Appl. Catal., A* **2001**, *222*, 427−437.
(7) Kung, M. C.; Davis, R. J.; Kung, H. H. *J. Phys. Chem. C* **2007**, *111*, 11767−11775.
(8) Haruta, M. *Faraday Discuss.* **2011**, *152*, 11−32.
(9) Wu, Y. Y.; Mashayekhi, N. A.; Kung, H. H. *Catal. Sci. Technol.* **2013**, *3*, 2881−2891.

(10) Fujitani, T.; Nakamura, I.; Haruta, M. *Catal. Lett.* **2014**, *144*, 1475−1486.

(11) Lopez, N.; Janssens, T.; Clausen, B.; Xu, Y.; Mavrikakis, M.; Bligaard, T.; Nørskov, J. K. *J. Catal.* **2004**, *223*, 232−235.

(12) Lopez, N.; Nørskov, J. K. *J. Am. Chem. Soc.* **2002**, *124*, 11262−11263.

(13) Remediakis, I. N.; Lopez, N.; Nørskov, J. K. *Angew. Chem.* **2005**, *117*, 1858−1860.

(14) Remediakis, I. N.; Lopez, N.; Nørskov, J. K. *Appl. Catal., A* **2005**, *291*, 13−20.

(15) Widmann, D.; Behm, R. J. *Acc. Chem. Res.* **2014**, *47*, 740−749.

(16) Kotobuki, M.; Leppelt, R.; Hansgen, D.; Widmann, D.; Behm, R. *J. Catal.* **2009**, *264*, 67−76.

(17) Widmann, D.; Behm, R. J. *Angew. Chem., Int. Ed.* **2011**, *50*, 10241−10245.

(18) Liu, Z.-P.; Gong, X.-Q.; Kohanoff, J.; Sanchez, C.; Hu, P. *Phys. Rev. Lett.* **2003**, *91*, 266102.

(19) Molina, L. M.; Rasmussen, M. D.; Hammer, B. *J. Chem. Phys.* **2004**, *120*, 7673−7680.

(20) Rasmussen, M. D.; Molina, L. M.; Hammer, B. *J. Chem. Phys.* **2004**, *120*, 988−997.

(21) Li, L.; Zeng, X. C. J. *J. Am. Chem. Soc.* **2014**, *136*, 15857−15860.

(22) Li, L.; Gao, Y.; Li, H.; Zhao, Y.; Pei, Y.; Chen, Z.; Zeng, X. C. *J. Am. Chem. Soc.* **2013**, *135*, 19336−19346.

(23) Wang, J. G.; Hammer, B. *Phys. Rev. Lett.* **2006**, *97*, 136107.

(24) Laursen, S.; Linic, S. *Phys. Chem. Chem. Phys.* **2009**, *11*, 11006−11012.

(25) Laursen, S.; Linic, S. *J. Phys. Chem. C* **2009**, *113*, 6689−6693.

(26) Vilhelmsen, L. B.; Hammer, B. *J. Chem. Phys.* **2013**, *139*, 204701.

(27) Vilhelmsen, L. B.; Hammer, B. *ACS Catal.* **2014**, *4*, 1626−1631.

(28) Wang, Y.-G.; Cantu, D. C.; Lee, M.-S.; Li, J.; Glezakou, V.-A.; Rousseau, R. *J. Am. Chem. Soc.* **2016**, *138*, 10467−10476.

(29) Wang, Y.-G.; Yoon, Y.; Glezakou, V.-A.; Li, J.; Rousseau, R. *J. Am. Chem. Soc.* **2013**, *135*, 10673−10683.

(30) Duan, Z.; Henkelman, G. *ACS Catal.* **2015**, *5*, 1589−1595.

(31) Wang, Y.-G.; Mei, D.; Glezakou, V.-A.; Li, J.; Rousseau, R. *Nat. Commun.* **2015**, *6*, 6511.

(32) Boccuzzi, F.; Tsubota, S.; Haruta, M. *J. Electron Spectrosc. Relat. Phenom.* **1993**, *64-65*, 241−250.

(33) Saavedra, J.; Powell, C.; Panthi, B.; Pursell, C. J.; Chandler, B. D. *J. Catal.* **2013**, *307*, 37−47.

(34) Denkwitz, Y.; Zhao, Z.; Hörmann, U.; Kaiser, U.; Plzak, V.; Behm, R. *J. Catal.* **2007**, *251*, 363−373.

(35) Diemant, T.; Bansmann, J.; Behm, R. *Vacuum* **2009**, *84*, 193−196.

(36) Daté, M.; Okumura, M.; Tsubota, S.; Haruta, M. *Angew. Chem., Int. Ed.* **2004**, *43*, 2129−2132.

(37) Gao, F.; Wood, T. E.; Goodman, D. W. *Catal. Lett.* **2010**, *134*, 9−12.

(38) Liu, L. M.; McAllister, B.; Ye, H. Q.; Hu, P. *J. Am. Chem. Soc.* **2006**, *128*, 4017−4022.

(39) Saavedra, J.; Doan, H. A.; Pursell, C. J.; Grabow, L. C.; Chandler, B. D. *Science* **2014**, *345*, 1599−1602.

(40) Bongiorno, A.; Landman, U. *Phys. Rev. Lett.* **2005**, *95*, 106102.

(41) Kresse, G.; Hafner, J. *Phys. Rev. B: Condens. Matter Mater. Phys.* **1993**, *47*, 558.

(42) Kresse, G.; Furthmüller, J. *Comput. Mater. Sci.* **1996**, *6*, 15−50.

(43) Kresse, G.; Furthmüller, J. *Phys. Rev. B: Condens. Matter Mater. Phys.* **1996**, *54*, 11169.

(44) Perdew, J. P.; Wang, Y. *Phys. Rev. B: Condens. Matter Mater. Phys.* **1992**, *45*, 13244.

(45) Blöchl, P. E. *Phys. Rev. B: Condens. Matter Mater. Phys.* **1994**, *50*, 17953.

(46) Dudarev, S. L.; Botton, G. A.; Savrasov, S. Y.; Humphreys, C. J.; Sutton, A. P. *Phys. Rev. B: Condens. Matter Mater. Phys.* **1998**, *57*, 1505−1509.

(47) Morgan, B. J.; Watson, G. W. *Surf. Sci.* **2007**, *601*, 5034−5041.

(48) Finazzi, E.; Di Valentin, C.; Pacchioni, G.; Selloni, A. *J. Chem. Phys.* **2008**, *129*, 154113.

(49) Henkelman, G.; Jónsson, H. *J. Chem. Phys.* **2000**, *113*, 9978−9985.

(50) Henkelman, G.; Uberuaga, B. P.; Jónsson, H. *J. Chem. Phys.* **2000**, *113*, 9901−9904.

(51) Bader, R. F. W. *Atoms in Molecules: A Quantum Theory*; Clarendon Press: Oxford, U.K., 1994; International Series of Monographs on Chemistry.

(52) Henkelman, G.; Arnaldsson, A.; Jónsson, H. *Comput. Mater. Sci.* **2006**, *36*, 354−360.

(53) Tang, W.; Sanville, E.; Henkelman, G. *J. Phys.: Condens. Matter* **2009**, *21*, 084204.

(54) Christmann, K.; Schwede, S.; Schubert, S.; Kudernatsch, W. *ChemPhysChem* **2010**, *11*, 1344−1363.

(55) Manchot, W.; Gall, H. *Ber. Dtsch. Chem. Ges. B* **1925**, *58*, 2175.

(56) Mihaylov, M.; Knözinger, H.; Hadjiivanov, K.; Gates, B. *Chem. Ing. Tech.* **2007**, *79*, 795−806.

(57) Goldman, A. S.; Krogh-Jespersen, K. J. *J. Am. Chem. Soc.* **1996**, *118*, 12159−12166.

(58) Bistoni, G.; Rampino, S.; Scafuri, N.; Ciancaleoni, G.; Zuccaccia, D.; Belpassi, L.; Tarantelli, F. *Chem. Sci.* **2016**, *7*, 1174−1184.

(59) Haynes, W. M. *CRC Handbook of Chemistry and Physics*, 97th ed.; CRC Press: Boca Raton, FL, 2016.

(60) Chase, M. W. J. *Thermochemical Tables*, 4th ed.; American Institute of Physics: New York, 1985.

(61) Boccuzzi, F.; Chiorino, A. *J. Phys. Chem. B* **2000**, *104*, 5414−5416.

(62) Boccuzzi, F.; Chiorino, A.; Manzoli, M.; Lu, P.; Akita, T.; Ichikawa, S.; Haruta, M. *J. Catal.* **2001**, *202*, 256−267.

(63) Raphulu, M. C.; McPherson, J.; van der Lingen, E.; Anderson, J. A.; Scurrell, M. S. *Gold Bull.* **2010**, *43*, 21−28.

(64) Henao, J. D.; Caputo, T.; Yang, J. H.; Kung, M. C.; Kung, H. H. *J. Phys. Chem. B* **2006**, *110*, 8689−8700.

(65) Widmann, D.; Krautsieder, A.; Walter, P.; Brückner, A.; Behm, R. J. *ACS Catal.* **2016**, *6*, 5005−5011.

(66) Maeda, Y.; Iizuka, Y.; Kohyama, M. *J. Am. Chem. Soc.* **2013**, *135*, 906−909.

(67) Kettemann, F.; Witte, S.; Birnbaum, A.; Paul, B.; Clavel, G.; Pinna, N.; Rademann, K.; Kraehnert, R.; Polte, J. *ACS Catal.* **2017**, *7*, 8247−8254.